THE AMERICAN SOCIETY OF MECHANICAL ENGINEERS
Three Park Avenue, New York, N.Y. 10016-5990

99-GT-194

UNSTEADY BOUNDARY LAYER TRANSITION ON A HIGH PRESSURE TURBINE ROTOR BLADE

Maik Tiedemann and **Friedrich Kost**
Institute of Fluid Mechanics
German Aerospace Center (DLR)
Göttingen, Germany

ABSTRACT

This investigation is aimed at the experimental determination of the location, the extent, and the modes of the laminar-to-turbulent transition processes in the boundary layers of a high pressure turbine rotor blade. The results are based on time-resolved, qualitative wall shear stress data which was derived from surface hotfilm measurements. The tests were conducted in the "Windtunnel for Rotating Cascades" of the DLR in Göttingen. For the evaluation of the influence of passing wakes and shocks on the unsteady boundary layer transition, a test with undisturbed rotor inlet flow was conducted in addition to full stage tests.

Two different transition modes led to a periodic-unsteady, multi-moded transition on the suction side. In between two wakes, transition started in the bypass mode and terminated as separated-flow transition. Underneath the wakes, plain bypass transition occurred. The weak periodic boundary layer features on the pressure side indicate that this surface was not significantly affected by passing wakes or shocks.

The acquired data reveals that the periodically disturbed suction side boundary layer is less susceptible to bubble bursting than the undisturbed flowfield. Thus, these blades may be subjected to higher aerodynamic loads. Accordingly, as in low pressure turbines, the unsteady effects in high pressure turbines may allow for a reduction of the number of rotor blades, with respect to the original design.

NOMENCLATURE

K	[ ]	acceleration parameter = $\nu/w^2\ dw/ds$
$\dot{m}$	[kg/s]	mass flow rate
$\dot{m}_{red}$	[kg $\sqrt{K}$/(s kPa)]	reduced mass flow = $\dot{m}\sqrt{T_{01}}/p_{01}$
N	[ ], [RPM]	number of evaluated rev., rotor speed
N_{red}	[1 / (min $\sqrt{K}$)]	reduced speed = $N/\sqrt{T_{01}}$
P	[mW]	CTA output power
p	[mW], [Pa]	power fluctuation value, pressure
r	[ ]	react. factor = $\dfrac{(p_2/p_{01})^{\frac{\gamma-1}{\gamma}} - (p_3/p_{01})^{\frac{\gamma-1}{\gamma}}}{1 - (p_3/p_{01})^{\frac{\gamma-1}{\gamma}}}$
s	[m]	surface length, s = 0 at the design stagnation point
T	[K]	Temperature
u	[m/s]	circumferential velocity
w	[m/s]	velocity in the relative frame
γ	[ ], [ ]	ratio of specific heats ($\gamma = c_p/c_v$), intermittency
ν	[m^2/s]	kinematic viscosity
τ_W	[N/m^2]	wall shear stress
Φ	[ ]	flow factor = axial velocity / circumfer. velocity
Ψ	[ ]	loading factor = $c_p\ (T_{03} - T_{01})/u_2^2$
Ω	[ ]	reduced frequency = $\dfrac{\text{axial rotor chord / axial vel.}}{\text{stator pitch / circumfer. vel.}}$

Subscripts

0	total condition, zero-flow condition
1, 2, 3	stator inlet, stator exit/rotor inlet, rotor exit
i, j	index along circumfer., index along revolutions
ps, ss	pressure side, suction side
p, r	periodic, random
w	in the relative frame of reference

Superscripts

~	ensemble-averaged value
–	time-averaged value

1. INTRODUCTION

While the turbomachine efficiencies of the first production jet engine - the Jumo 004 - were below 80%, the efficiency of many large machines is nowadays over 90%. Consequently, further improvements in efficiency and performance have become progressively more difficult.

An improvement of the thrust-to-weight ratio of an engine by means of an increase in thrust would require an increase in turbine inlet temperature. This would result in higher thermal loads on the turbine blades, which already operate at temperatures above the melting point of the blade materials. Therefore, thorough information on the turbine heat transfer is needed to enable the design of efficient cooling systems

Presented at the International Gas Turbine & Aeroengine Congress & Exhibition
Indianapolis, Indiana — June 7–June 10, 1999

(particularly in high pressure turbines). Improving the thrust-to-weight ratio by means of a weight reduction can be obtained by reducing the number of stages or blades of an engine's turbomachinery components. However, the resulting higher aerodynamic loads on the remaining blades lead to an increase in diffusion, which may result in an unacceptable increase in losses due to non-reattached flow.

Traditionally, turbomachinery components have been designed and tested under steady-state conditions. However, due to the relative motion of the blade rows, the actual flowfield is unsteady. Recent advances in fast response instrumentation, as well as advances in computational techniques and computer power, have led to results which indicate that unsteady effects represent a potential for an increase in jet engine efficiency. Since heat transfer in turbulent boundary layers is three to five times larger than in laminar boundary layers, laminar-to-turbulent transition plays a significant role in heat transfer. It is generally accepted that transition on gas turbine airfoils is unsteady and that wakes and shocks, shed by upstream blades, can promote transition ahead of the respective positions in undisturbed inlet flow. Investigations of low pressure turbines have revealed evidence that unsteady boundary layer effects may lead to an increased diffusion capability of turbomachinery blades (Halstead et al., 1997, Hodson, 1998). Thus, the heat transfer distribution, as well as the mechanisms which rule the diffusion capability of a turbine blade, are related to unsteady boundary layer phenomena. Furthermore, boundary layer transition directly influences the blade profile losses, and thus the turbine efficiency. Hodson (1983) observed that the profile loss on a turbine rotor with wake disturbed inlet flow was 50% higher than with undisturbed inlet flow.

Due to the need for fast response measurement techniques and powerful data acquisition and evaluation systems, the systematic investigation of periodic-unsteady boundary layer effects began only in the seventies (see e.g. Walker, 1974). Based on results which were obtained in a simulated turbomachinery environment (flat plate with bar wake generator) Pfeil et al. (1983) stated that transition in these machines is a wake-induced, periodic-unsteady process. They introduced a transition model that is based on the periodic occurrence of wake-induced turbulent spots in an otherwise laminar flow. Hodson's (1983) large-scale, low-speed turbine stage results are in very good agreement with this model. Many researchers investigated different aspects of wake-induced transition processes in large-scale facilities, e.g. Dring et al. (1982), Sharma et al. (1988), Addison and Hodson (1990), and only recently Halstead et al. (1997). The latter investigation indicated that wakes may suppress laminar separation, and that becalmed regions may result in laminar-like attached flow downstream of the nominal separation point. The recognition of these facts resulted in a weight reduction of modern low pressure turbines due to a reduction of the number of blades per row with increased individual blade loads. Thus, the investigation of periodic-unsteady transition processes has resulted in an improvement in gas turbine efficiency. However, the question of whether these results are applicable to the transonic, high Reynolds number flowfields of high pressure turbines (HPT) calls for further investigations.

Even though some important aspects of transonic HPT flowfields have already been investigated (e.g. the effects of incident shocks, Doorly and Oldfield, 1985 and Guenette et al., 1989), the designer still has questions about the structure of the boundary layers in these machines. In order to make a contribution to the investigation of these important issues, the present work is aimed at the determination of the periodic-unsteady boundary layer transition pattern on the rotor blades of a transonic aero-engine high pressure turbine. In order to keep the complexitity of this investigation in this very challenging environment within reasonable limits, an internally cooled stator / uncooled rotor configuration was chosen. Since most first stage blade rows are film cooled, this can only be seen as a first step towards the determination of the boundary layer conditions in a real engine HPT. However, the investigated conditions are representative of typical second stage blade rows. Hodson (1985) observed the relaminarization of turbulent spots which had developed as a result of a flow separation in an "overspeed" region close to the blade leading edge. Rotor suction surface film cooling is typically restricted to the leading edge region of a blade. Thus, turbulent spots which are induced by film cooling jets may relaminarize as well. In this case, the present results would also be applicable to first stage rotors (at least in the more important rear part of the blade).

2. EXPERIMENTAL APPARATUS

2.1 The "Windtunnel for Rotating Cascades" (RGG)

The RGG is a closed circuit, continuously running windtunnel (see **Figure 1**). A four stage radial compressor (maximum pressure ratio: 6) driven by a speed-controlled 1 MW dc-motor provides a volume flow rate of up to 15.5 m^3/s. All components of the facility are accurately controlled by means of a "Simatic S5" industrial control system.

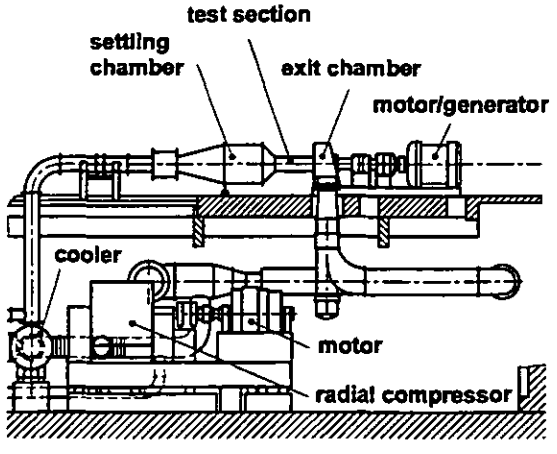

Figure 1: Sketch of the RGG

Possible rotor speeds are up to 10,000 RPM in both directions. The rotor is coupled to a speed-controlled 500 kW dc-motor/generator which can drive or brake the rotor in either direction. The entire start-up procedure of the windtunnel lasts approximately 45 minutes which leads to adiabatic conditions around the blades by the time the actual tests are started. An auxiliary compressor (with a downstream cooler) provides air for the simulation of stator coolant ejection.

For a choked stator (typical for HPTs), the stage inlet Mach number is determined by the vane geometry. The stator exit Mach number is coupled to the rotational speed of the main compressor which determines the static pressure downstream of the stator throat, i.e. for a given settling chamber pressure, the stage pressure ratio is controlled by the compressor speed. The Reynolds number depends mainly on the adjustable settling chamber pressure and temperature levels. Thus, Mach and Reynolds number can be varied independently within certain limits.

The stator inlet turbulence level is approximately 1.5% which is very small for an HPT flowfield. However, Blair et al. (1988) observed

that, even though the effect of changes in inlet turbulence is dramatic on the stator heat transfer, it is almost negligible on the rotor heat transfer and, thus, on the rotor boundary layer transition. This observation was attributed to the fact that the rotor flowfield disturbances are due to the unsteadiness (wakes and shocks) generated by the stator, rather than to the inlet turbulence. Therefore, this shortcoming of the facility does not necessarily decrease the applicability of the results.

2.2 The turbine stage

The investigated turbine stage was designed by Alfa Romeo Avio (Santoriello et al. 1993) in the course of the IMT Area 3 turbine project. It comprises a state-of-the-art, full size, transonic, aero-engine HPT. In order to keep the complexity within reasonable limits, this investigation was restricted to the blade mid-span region. The blade row geometry is given in **Table 1**. **Figure 2** shows the stage and the positions of the hotfilm gauges (20 suction side and 14 pressure side gauges).

Table 1: Geometrical parameters of the turbine blade rows

	Stator	Rotor
Axial chord c_{ax}	29.86 mm	27.45 mm
Tip radius	274.00 mm	274.00 mm
Hub radius (inlet)	238.84 mm	238.84 mm
Aspect ratio (inlet)	0.71	1.07
Stagger angle	51.90 °	32.71 °
Number of blades	43	64

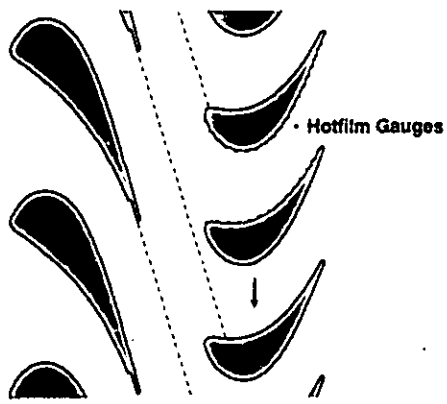

Figure 2: Stage configuration at mid-span

2.3 Measurement technique and data acquisition

The utilized surface hotfilm technique is very similar to hot wire anemometry. The power required to keep the hotfilm resistance (and thereby the temperature) constant depends on the heat transfer towards the fluid which is related to the wall shear stress. The gauge overheat temperature was set to 60 K by soldering fixed resistances into the adjust arm of the Wheatstone bridge. The cut-off frequency of the gauges (determined by means of a Fourier analysis) of approximately 15-20 kHz is significantly larger than the value of 10 kHz given by the gauge manufacturer MTU Munich. This frequency response was sufficient to resolve the first three harmonics of the vane passing frequency (5.66 kHz) for most of the gauges (see Tiedemann, 1998 for details).

The signals from the hotfilm gauges (which were glued onto the rotor surfaces) were processed by rotating constant temperature anemometers (CTA). Up to 20 gauges can be connected to each of the two CTA boards. The gauges and their respective adjust resistors were successively switched into the CTA bridge. Since the data of the different gauges was not sampled simultaneously, the tracking of flow features in the raw data traces is not possible. For this reason, the presentation of raw data traces is omitted. Voltage to frequency conversion circuits convert the analog CTA output voltage into a TTL pulse train. An optoelectronic system was used to transmit these pulses to the stationary frame of reference. The CTAs and the transmission system were developed by the University of Limerick (see Davies et al., 1997 for details).

A shaft encoder triggers the PC-based A/D converter. Afterwards, exactly one sample is taken for each of the 1024 pulses the encoder delivers per revolution. This technique guarantees that the samples are taken at the same stator-rotor position in every revolution, which is beneficial for the ensemble-averaging technique described below.

3. DATA EVALUATION

Prior to the actual data evaluation, the sampled signals were corrected for offset errors (DC), and phase shift and attenuation errors (AC). According to Bellhouse and Schultz (1966), the voltage drop over the gauge V is related to the wall shear stress τ_W by :

$$\frac{V^2}{R} - \frac{V_0^2}{R_0} = P - P_0(\Delta T) = a\tau_W^{\frac{1}{3}}\Delta T \qquad (1)$$

The resistance R, and thereby (for a given surface temperature) the hotfilm overheat temperature ΔT, is set by means of the above-mentioned adjust resistor. P_0 is the dissipated power at zero-flow. Since the surface temperatures at zero-flow and during the actual test differed significantly, calibration curves for P_0 vs. ΔT had to be determined.

Since the calibration of hotfilm gauges is complicated and subject to errors, the determination of the boundary layer state is often based on the qualitative relation between the hotfilm signal and the wall shear stress (see e.g. Schröder, 1991). The effects of possible manufacturing differences of the gauges (normally contained in "a") can be eliminated by normalizing the signals with P_0 (Schröder, 1991). Thus, the parameter $(P - P_0) / P_0$, which is used throughout this paper, is proportional to $\tau_W^{1/3}$ and enables the comparison of signals from different gauges.

In order to separate the periodical signal components from the random components, the ensemble-averaging technique (EA) was applied. This technique averages the data of the 448 sampled revolutions at fixed stator/rotor phase angles (given by the 1024 encoder pulses). The EA hotfilm signal is obtained from :

$$\bar{P}_i = \frac{1}{N}\sum_{j=1}^{N} P_{ij} \quad ; \qquad i = 0...1023,\ N = 448 \qquad (2)$$

Ideally, the random components are averaged out in the resulting periodic-unsteady signal. The EA random unsteadiness :

$$p_{r,i} = \sqrt{\frac{1}{N-1}\sum_{j=1}^{N}(P_{ij} - \bar{P}_i)^2} \qquad (3)$$

is a measure of non-periodic effects, i.e. effects which are not directly connected to vane passings. Theoretically p_r would include turbulence

effects. However, the characteristic turbulence frequency in the investigated stage is in the order of 300 kHz and, thus, much higher than the cut-off frequency of the gauges (approximately 15-20 kHz).

The ensemble-averaged skewness :

$$\text{Skewness}_i = \frac{1}{(p_{r,i})^3}\frac{1}{N}\sum_{j=1}^{N}(P_{ij} - \bar{P}_i)^3 \qquad (4)$$

is a non-dimensional number which proved very helpful in the discussion of the time-resolved data.

The above described parameters were then circumferentially averaged to obtain time-averaged values, i.e.: the 1024 values per gauge were further reduced to a single value per gauge.

The time-averaged periodic fluctuations :

$$\bar{p}_p = \sqrt{\frac{1}{T}\int_0^T (\bar{P}(t) - \bar{P})^2\,dt} \qquad (5)$$

are an integral measure for the overall periodic unsteadiness of the signal during the period T (e.g. wake and shock induced unsteadiness).

4. TEST PARAMETERS

The operating parameters of the stage are given in **Table 2**. The error margins in the determination of pressures are in the order of 0.1% of the measured value, temperatures are determined within ± 0.3 K, N is accurate to within ± 1 RPM and the error in the mass flow is about 1% of the measured value. The Mach number values in **Table 2** have accuracies of approximately ± 0.004, while the contour Mach numbers presented in **Figures 3** and **4** are only accurate to within ± 0.01 (due to additional extrapolation errors). The Reynolds number Re_2 is based on stator exit conditions and stator chord, while Re_{w3} is based on rotor exit conditions in the relative frame of reference and rotor chord. The presented parameters characterize the investigated stage as representative of a small to mid-size aircraft engine HPT. Laser-2-Focus velocimeter (L2F) measurements revealed the occurrence of weak stator trailing edge shocks, despite the subsonic mean stator exit Mach number.

The stator vanes are equipped with coolant ejection slots at the pressure side, close to the trailing edge (see **Figure 2**). Tests were conducted with no coolant ejection and with the design ejection of 3% of the main mass flow. In addition, two inter-blade row gaps (0.49 and 0.38 $c_{ax,Stator}$) were investigated. Since no noticeable changes in the boundary layer behaviour were observed between the different tests (see Tiedemann, 1998 for details), only the results of the 3% coolant ejection, 0.49 $c_{ax,Stator}$ gap stage test are presented in this paper.

In order to enable the evaluation of the influence of passing wakes and shocks on the unsteady boundary layer transition, a test with undisturbed rotor inlet flow was conducted in addition to full stage tests. For this purpose, the stator was removed (resulting in axial inlet flow) and the rotor was driven (reversed operation with respect to the nominal direction of rotation) so that the mid-span Mach number triangles of the stage tests were correctly reproduced. Since the tip was sealed by an abradable material, no tip flows occured. The mid-span conditions in the relative frame of reference were very similar in the two test cases (see Tiedemann, 1998 for details). Only the Reynolds number in the rotor only test had to be reduced by 10% (due to torque restrictions).

The rotor Mach number distributions of the two configurations are presented in the next section (see **Figures 3** and **4**). The solid lines in these figures represent the design Mach number distribution (computed by Santoriello et al., 1993). The data points in these figures were obtained by extrapolating L2F velocity data to the boundary layer edge (see Kost and Kapteijn (1997) for details of the L2F system and the data evaluation). The distributions are in excellent agreement on the pressure side and in very good agreement on the rear part of the suction side, where most of the boundary layer transition occurs.

Table 2: Basic operating parameters of the turbine stage

absolute stator exit Mach number M_2	0.937
relative rotor exit Mach number M_{w3}	0.938
absolute stator exit Reynolds number Re_2	$0.866 \cdot 10^6$
relative rotor exit Reynolds number Re_{w3}	$0.396 \cdot 10^6$
relative rotor inlet angle β_2	40.9°
relative rotor exit angle β_3	−56.1°
rotor speed N [1 / min]	7894
reduced speed N_{red} [1 / (min $K^{1/2}$)]	447.4
reduced mass flow $\dot{m}_{red}$ [kg $K^{1/2}$ / (s kPa)]	0.665
stage reaction factor r	0.454
stage loading coefficient Ψ	1.519
stage flow factor Φ	0.431
reduced frequency Ω	1.23

5. RESULTS AND DISCUSSION

5.1 Rotor pressure side

The time-averaged surface hotfilm signals of the rotor pressure side are presented in **Figure 3** for both test configurations. Downstream of a region of almost constant shear stress, which ends around $s/s_{max,ps} = 0.21$, the time-averaged hotfilm signal in the top plot indicates a steady increase in wall shear stress. This pattern can be attributed to the acceleration along the pressure surface. Due to the constant velocity (see the Mach number distribution in the bottom plot of **Figure 3**), the wall shear stress in the leading edge region was relatively constant. The strong acceleration in the rear part of the pressure side coincides with the observed increase in wall shear stress.

Neither the time-averaged random fluctuations presented in the second plot of **Figure 3**, nor the time-averaged skewness given in the third plot, show any sign of boundary layer transition. Since the gauge at the leading edge was damaged prior to the tests, it is not possible to determine whether or not the boundary layer transitioned upstream of the first active gauge. However, even though the acceleration parameter K in the rear portion of the pressure side of approximately $6 \cdot 10^{-6}$ is well in excess of the critical value for relaminarization of $3 \cdot 10^{-6}$, there is no evidence of reverse transition in the data. Thus, it can be concluded that the pressure side boundary layer remained entirely laminar.

Apart from the large periodic fluctuations in the leading edge region, the plots do not indicate any significant change in the boundary layer data of the stage test with respect to the rotor only test, i.e. the pressure side boundary layer seems to have remained largely unaffected by the wakes and shocks associated with the presence of the stator.

5.2 Rotor suction side, time-averaged results

Figure 4 shows the time-averaged suction side results of the rotor only test. Considering the strong acceleration upstream of $s/s_{max,ss} = 0.21$ (region of failed gauges), it can be assumed that the

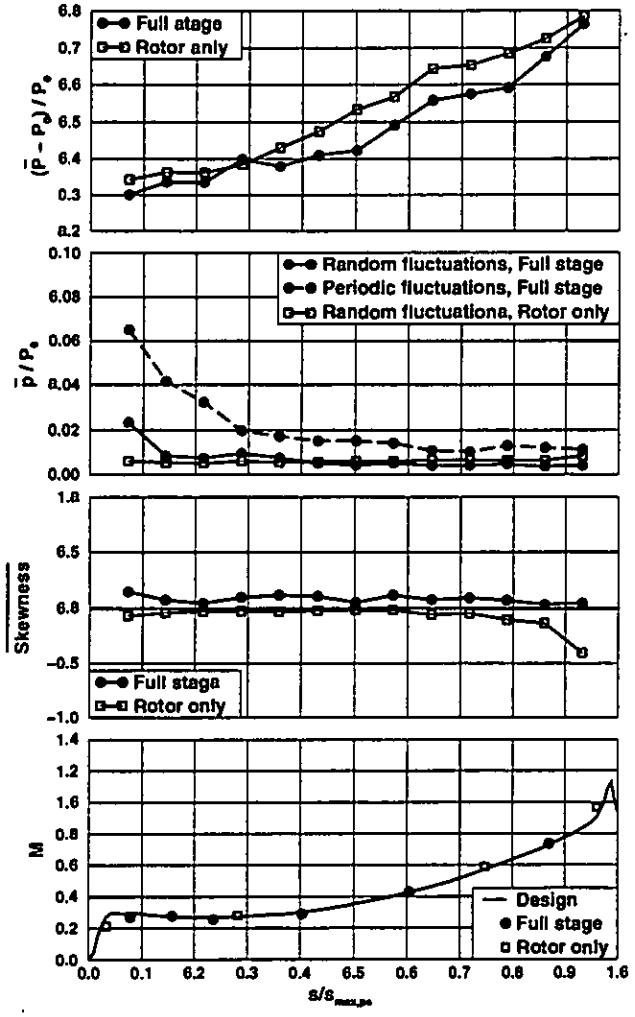

Figure 3: Time-averaged hotfilm data and Mach number distribution; pressure side, rotor only and full stage

boundary layer was laminar in this region. Since over the first half of the suction surface neither the random fluctuations $\bar{p}_r$ / P_0 nor the skewness show any sign of transition onset, it is apparent that the boundary layer remained laminar upstream of $s/s_{max,ss} = 0.5$.

As a result of the shock / boundary layer interaction, suction side transition in transonic turbines usually includes the formation of a shock-induced separation bubble. Since the wall shear stress vanishes at a separation point, $(\bar{P} - P_0) / P_0$ should actually vanish as well. However, as the gauges were used in a qualitative manner, it is not likely that the traces actually approach zero at separation, but it can be expected that they show a minimum. Due to the unsteady motion of the passage shock, the separation bubble and, thus, the separation point oscillates in the streamwise direction. Therefore, the time-averaged shear stress at the time-mean separation point is averaged over shear stress levels from upstream and inside the bubble. For this reason, the time-averaged wall shear stress minimum occurs where the gauges are permanently located inside the bubble which is downstream of the time-mean separation point. This effect was reported by Kost et al. (1988), who compared plane cascade, time-averaged hotfilm data to schlieren pictures and oil-flow visualizations. Therefore, the top plot of **Figure 4** indicates a possible separation region in the vicinity of $s/s_{max,ss} = 0.7$.

This hypothesis is supported by the time-averaged random fluctuations (second plot of **Figure 4**). The first fluctuation peak is most likely due to the unsteady motion of the separation point, while the higher peak at $s/s_{max,ss} = 0.89$ results only partly from reattachment point oscillations. Large portions of this peak must be attributed to the intense transitional activity (frequent changes between laminar and turbulent flow) which occurs shortly upstream of the (usually) turbulent reattachment. The results of Kost et al. (1988) confirm the connection between the observed double peak pattern and a bubble. Thus, the fluctuation plot indicates a separation bubble that originates at $s/s_{max,ss} = 0.63$ and ends somewhat downstream of $s/s_{max,ss} = 0.89$. Since even a laminar boundary layer can take some diffusion prior to separation, the coincidence of the separation point and the pressure minimum (Mach number maximum) must be considered a mismatch between the (numerical) Mach number distribution and the hotfilm data.

The intermittency γ describes the fraction of time during which the flow at a certain position is turbulent. In the absence of any random disturbances a flat time-resolved signal (e.g. pure laminar flow, $\gamma = 0$; or pure turbulent flow, $\gamma = 1$) results in zero skewness. For $\gamma = 0.25$ the skewness reaches its maximum. At $\gamma = 0.5$, where equal periods of laminar and turbulent flow exist, it decreases to zero (this point coincides typically with the random fluctuation maximum, as indicated by the dashed line ("$\gamma = 0.5$") in **Figure 4**). At $\gamma = 0.75$ the skewness exhibits a minimum (see e.g. Halstead et al., 1997, Part 2). Note, that signal noise and other random effects (e.g. shock oscillations) may lead to a noisy and messy skew distribution which deviates significantly from the described ideal distribution. However, the skewness plot in **Figure 4** indicates a transition cycle between $s/s_{max,ss} = 0.7$ and 1. The upward shift of the trace was probably caused by the superposition of the laminar / turbulent fluctuations and the reattachment point motions. The skewness minimum at $s/s_{max,ss} = 0.58$ was possibly caused by extreme forward motions of the separation bubble (similar motions have been observed by Kost et al., 1988 in a plane cascade facility).

The decrease of the random fluctuations downstream of their maximum and the increase in skewness downstream of its minimum indicate the completion of transition. Since a separated shear layer reattaches shortly after transition, it can be assumed that the flow reattached shortly upstream of the trailing edge. The end of the "bubble" region in **Figure 4**, was drawn in a somewhat arbitrary position, because the exact reattachment position cannot be determined from the available data.

Summing up, under undisturbed rotor inlet conditions the suction side boundary layer was laminar and attached on the forward portion of the blade. Laminar separation took place in the vicinity of $s/s_{max,ss} = 0.63$, and turbulent reattachment occurred slightly upstream of the blade trailing edge.

Figure 5 shows the time-averaged results of the full stage test. Following the above discussion, the qualitative wall shear stress data in the top plot indicates laminar flow up to $s/s_{max,ss} = 0.63$. The minimum downstream of this region coincides with the impingement point of the passage shock, which almost certainly caused the flow to separate, i.e.: it triggered the typical shock-boundary layer interaction. Hummel (1998) confirmed the shock impingement location in a numerical investigation.

The maximum in the time-averaged random fluctuations as well as the pattern of the time-averaged skewness indicate, that in the time-mean the line of 50% intermittency (labelled "$\gamma = 0.5$" in **Figure 5**) was located slightly downstream of the wall shear stress minimum. As

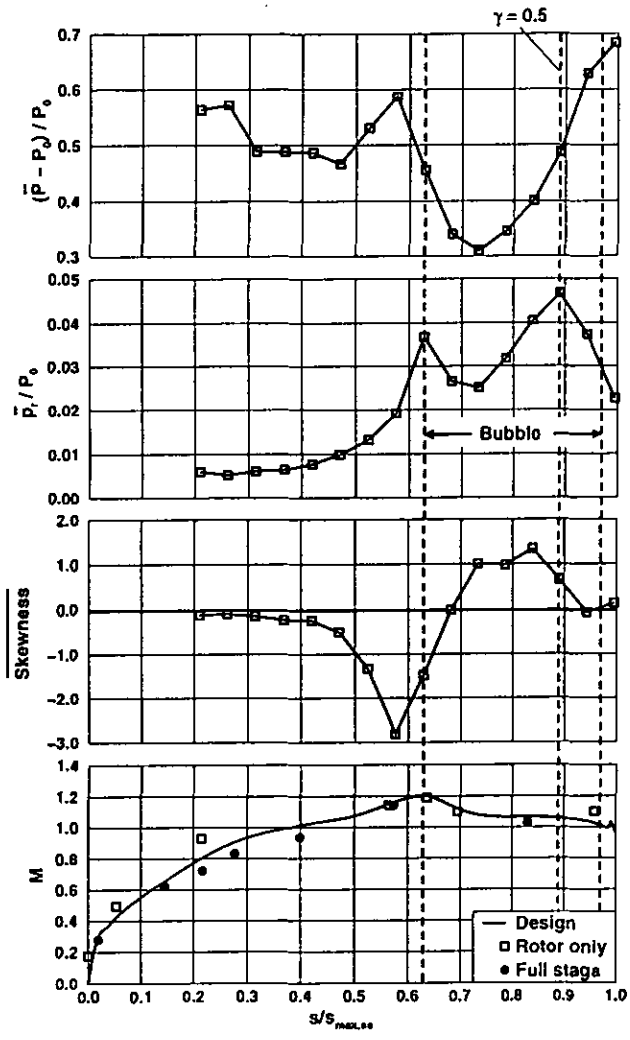

Figure 4: Time-averaged hotfilm data; suction side, rotor only; and suction side Mach number distributions

mentioned above, a separation bubble causes a double peak pattern in the random fluctuation plot. For the small bubble in this case these two peaks coincided to form one broad peak (around $s/s_{max,ss} = 0.7$). The high level of periodic fluctuations at this position indicates that the motions (and possibly the occurrence) of the bubble were coupled to the stator vane passing frequency, i.e.: they were caused by the periodic appearance of wakes or shocks. The periodic fluctuations show some additional cyclic activity in the region between $s/s_{max,ss} = 0.35$ and 0.55. In this region, the random fluctuations show slightly increased values as well and the skewness shows a broad maximum. The discussion of the time-resolved values will show that these phenomena were due to a second transitional region. Apparently, the suction side transition cannot be determined from the time-averaged data alone.

The low fluctuation level and the zero skewness downstream of $s/s_{max,ss} = 0.84$, indicate a fully turbulent boundary layer, i.e. transition in the full stage test was completed well upstream of the blade trailing edge. In addition, the bubble appears significantly smaller than in the rotor only case.

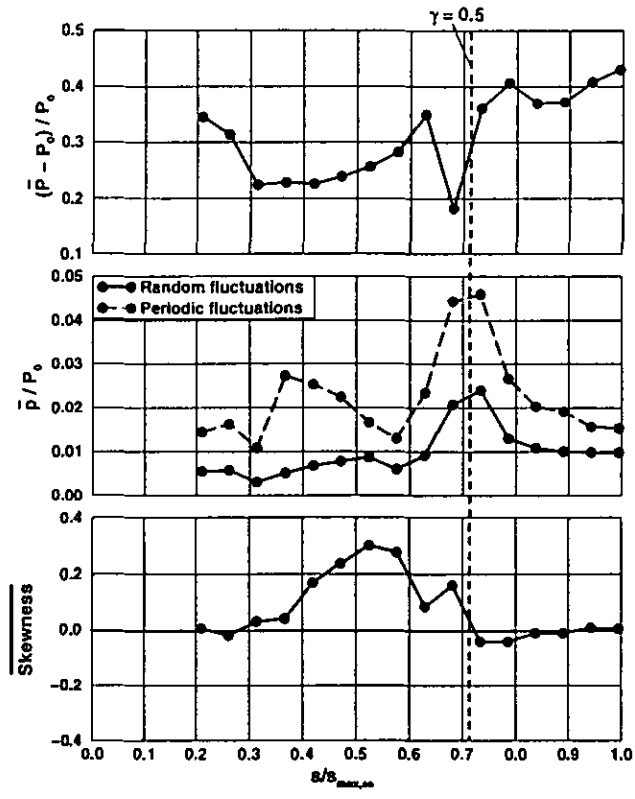

Figure 5: Time-averaged hotfilm data; suction side, full stage

5.3 Rotor suction side, time-resolved results

As mentioned above, the transition mechanisms in the full stage test cannot be deduced from the time-averaged data alone. Due to the fact that the transition phenomena are coupled to the periodic-unsteady occurrence of wakes and shocks, the ensemble-averaged time-resolved data is much more appropriate for the investigation of turbomachinery transition processes. Since the time-resolved pressure side results did not show any additional phenomena (with respect to the time-averaged results), they are not presented here.

Doorly and Oldfield (1985) observed that stator trailing edge shocks trigger a turbulent spot on the forward portion of the blade. While the direct shock effect is swept upstream, the shock-induced turbulent spot propagates downstream much like a wake-induced spot. Guenette et al. (1989) confirmed the occurrence of this effect in a transonic HPT rig. In the investigated stage configuration, the stator shocks would have impinged on the suction side in between the wakes. Thus, it should have been possible to identify the effects of shock-induced turbulent spots. The fact that no evidence of additional spots was found indicates that the effect of these shocks was negligible. Either, the shocks did not lead to transition at all, or the turbulent boundary layer relaminarized upstream of the first active gauge. However, even though stator shock effects did not occur here, they may well occur at a higher stator exit Mach number (and the associated increased shock strength).

Figure 6 shows time-distance contour plots of the ensemble-averaged hotfilm signal, random unsteadiness, and skewness of the full stage suction side test. The lines in these figures represent turbulent spot leading edge trajectories at 88% of the freestream velocity, according to Schubauer and Klebanoff (1955). Even though this is a zero pressure

gradient, incompressible flow value, it was chosen here because it comprises a reasonable compromise in the published range of leading eade velocities (see Tiedemann, 1998 for a discussion). The wake trajectory (labelled "a") was detected as the path along which the random fluctuations showed the earliest increase (due to the intense fluctuations in the wake).

Like the time-averaged signals, the time-resolved signals show no sign of transition on the forward portion of the blade. As mentioned above, random fluctuations show a distinct maximum at the location of 50% intermittency. Thus, the regions labelled "A" and "B" in the center plot of Figure 6 are possible locations of intense transitional activity. Apparently, the onset of transition along the wake path (trajectory "a", passing over region "A") took place well upstream of the transition onset in between wakes (trajectory "b", region "B").

In the skewness plot at the bottom of Figure 6, the regions "A" and "B" are (like in the fluctuation plot) located in regions of 50% intermittency (zero skewness). The sinusoidal yellow line (zero skewness) around $s/s_{max,ss} = 0.6$ marks the changing transition locations. The fact that the frequency of this line coincides with the stator vane passing frequency confirms that the boundary layer transition on the rotor suction surface was periodically altered by stator vane effects.

The flow over region "A" was dominated by wake effects and the high level of turbulence connected to them (the L2F data reveals turbulence levels in excess of 10%). Due to this high degree of turbulence it is more than reasonable to assume bypass transition along the wake-affected path.

The blue spots in the shear stress contours (top plot) slightly upstream of ($s/s_{max,ss} = 0.7$) indicate an increased intensity of the shock-boundary layer interaction in between wakes (Region "B"). As discussed below, these blue spots were caused by a small separation bubble. Since the flow downstream of this bubble was turbulent, the bubble was part of a separated-flow transition process.

The data presented in Figure 7 was extracted from Figure 6 along the drawn turbulent spot leading edge trajectories. The distinct features of the data set corresponding to the flow between wakes (trajectory "b" in Figure 7) are :

- large downward peak of the hotfilm signal in the shock-boundary layer interaction region ($s/s_{max,ss} = 0.7$)
- one large peak in the p_r/P_0 signal at $s/s_{max,ss} = 0.7$
- zero skewness at approximately $s/s_{max,ss} = 0.7$

The particular features of the data set corresponding to the wake-affected flow (trajectory "a") are :

- very low hotfilm values around $s/s_{max,ss} = 0.4$
- small downward peak of the hotfilm signal in the shock-boundary layer interaction region
- two peaks in the p_r/P_0 signal at $s/s_{max,ss} = 0.5$ and 0.7
- zero skewness at $s/s_{max,ss} = 0.5$ (see also Figure 6)

The onset of transition in between the wakes (trajectory "b") is marked by the skewness increase around $s/s_{max,ss} = 0.5$. Around $s/s_{max,ss} = 0.64$, the intermittency had reached 25% (skewness maximum). The maximum in the random fluctuations p_r/P_0 and the zero-crossing of the skewness indicate that the intermittency reached 50% in the shock-boundary

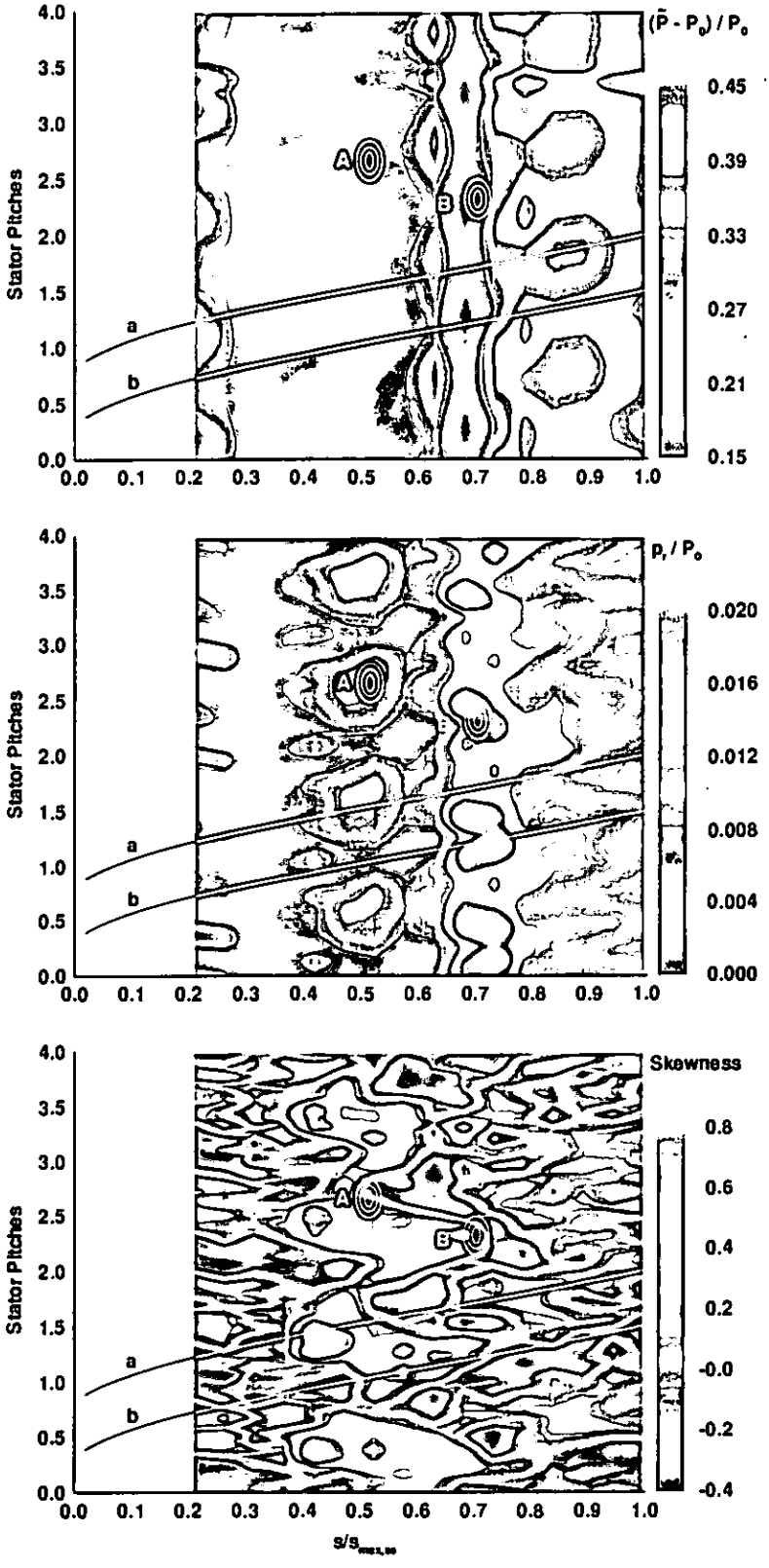

Figure 6: Qualitative wall shear stress, random fluctuation, and skewness contours; suction side, full stage

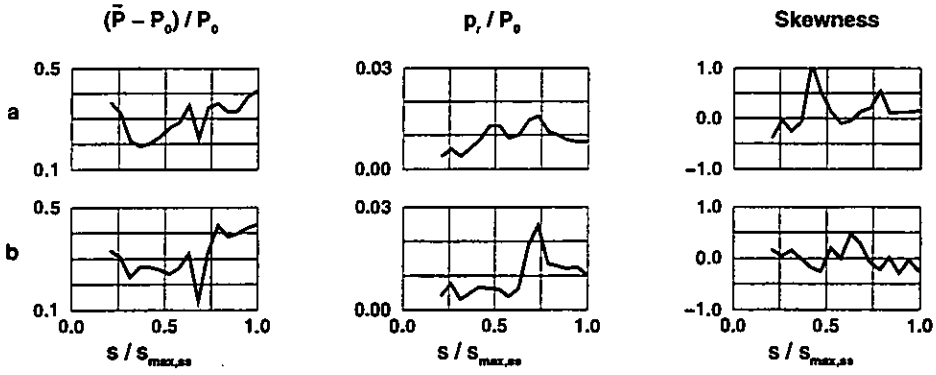

Figure 7: Comparison of hotfilm data extracted from Figure 6 along trajectories "a" and "b"; suction side, full stage

layer interaction region around $s/s_{max,ss} = 0.7$. At $s/s_{max,ss} = 0.77$, the intermittency along trajectory "b" had already increased to 75% (skewness minimum). Since neither the intermittent changes between laminar and turbulent flow, nor separation bubble oscillations occur in the turbulent branch, the decreased random fluctuations downstream of $s/s_{max,ss} = 0.8$, indicate the completion transition. Note, that the locations of the characteristic intermittency values are only approximate (due to the fact that skew is very sensitive to random disturbances).

The blue spots around $s/s_{max,ss} = 0.7$ in the top plot of **Figures 6**, as well as the traces in **Figure 7** indicate a more pronounced shock-boundary layer interaction in between two wakes (region "B", trajectory "b"), as compared to the wake-affected path. Since the actual shock effect is extremely short, these spots indicate the occurrence of a small (shock-induced) separation bubble. The increased random fluctuation maximum along this path can be attributed to additional fluctuations due to shock-induced bubble oscillations. A shock may interact with a turbulent boundary without forming a noticeable separation bubble. The quite pronounced bubble in between wakes indicates, therefore, that the boundary layer was either laminar or transitional before it encountered the interaction with the passage shock. The location of transition onset (increase in skew) was located well upstream of the identified separation bubble, i.e. the boundary layer was already transitional when it separated. From the L2F data, it is known that the turbulence intensity between the wakes was well above 1%, which is considered the lower limit for the occurrence of bypass transition. The decreased random fluctuations around $s/s_{max,ss} = 0.8$ were interpreted as an indication for a turbulent boundary layer. Thus, slightly downstream of the detected bubble, the boundary layer flow was turbulent. This means that the transition "mode" between wakes was a combined mode which started in the attached boundary layer as bypass transition and terminated via a small shock-induced bubble as separated-flow transition.

The onset of transition along the wake-affected path is indicated by the skewness increase around $s/s_{max,ss} = 0.37$ along trajectory "a" in **Figure 7**. It is well-known that boundary layers thicken under the influence of passing wakes. Thus, it appears reasonable that the low hotfilm values observed around $s/s_{max,ss} = 0.4$ along trajectory "a", were caused by the wake-induced thickening of the boundary layer. Around $s/s_{max,ss} = 0.42$, the intermittency along the wake-affected path ("a"), had reached 25% (skewness maximum). The first fluctuation maximum and the zero skewness around $s/s_{max,ss} = 0.5$ mark the location of 50% intermittency. In the vicinity of 62% surface length, the intermittency had increased to 75% (skewness minimum). Thus, underneath the wake, transition did not occur immediately at the wake impingement point (as assumed in Mayle and Dullenkopf's (1990) turbulent strip theory), but extended over a finite length. The random fluctuation reduction around $s/s_{max,ss} = 0.65$ indicates that the wake-induced transition was completed upstream of the shock impingement region ($s/s_{max,ss} = 0.7$). The second maximum in the random fluctuation plot is, thus, due to a (typically weak) shock / turbulent boundary layer interaction.

The two local maxima in the time-averaged periodic fluctuations in **Figure 5**, are located in the immediate vicinity of intense transitional activity which is a further indication for the fact that the transition modes were coupled to stator vane passing events. The observed broad time-averaged skewness maximum was caused by the periodical shift of the transition region.

6. CONCLUSIONS

The rotor suction side transition and separation locations are summarized in **Figure 8**. Under undisturbed rotor inlet conditions, separated-flow transition occurred including an extended bubble. In the full stage test, two different transition modes were detected which alternated at the vane passing frequency and formed a periodic-unsteady multimoded transition process. In between two wakes, transition started around $s/s_{max,ss} = 0.5$ and was completed around $s/s_{max,ss} = 0.8$. The process started as bypass transition and was terminated via a shock-induced separation bubble. Along the stator wake-affected path, the wake turbulence initiated bypass transition at approximately $s/s_{max,ss} = 0.37$ and transition was completed slightly upstream of the shock-boundary layer interaction region ($s/s_{max,ss} = 0.7$). Note that, in contrast to the rotor only test case, the transition processes in the stage test were completed well upstream of the blade trailing edge.

Between two wakes transition started significantly earlier than under undisturbed inlet conditions. During wake-induced transition, the intermittency at the location of transition onset along the path in between wakes was approximately 50%. Transition between wakes may, therefore, have been triggered by "residuals" of the wake-induced transition. This would mean that the boundary layer needed a certain time to recover from the wake-induced transition. The fact that transition in between wakes started upstream rather than downstream of the respective position in the undisturbed inlet flow case, indicates that becalmed regions did not exist in the investigated configuration.

The major difference between the two investigated cases is the larger separation bubble under undisturbed inlet conditions. This bubble originated slightly downstream of the pressure minimum and extended almost to the trailing edge. The flow at the separation point was entirely

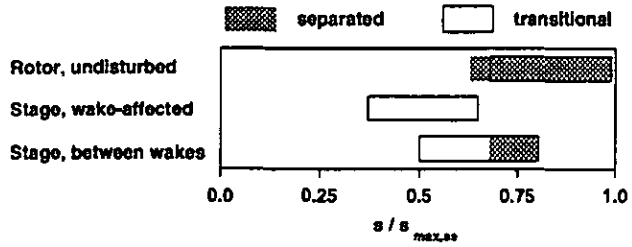

Figure 8: Comparison of separation and transition regions

laminar and transition started in the separated shear layer. For the full stage test, the flow between wakes was already intermittent at the separation point. This led to a soon breakdown to turbulence which caused the shear layer to reattach significantly earlier than in the rotor only test.

In order to save on engine weight and manufacturing costs, it is desirable to reduce the number of blades per blade row or even the number of stages (without reducing the work output). This reduction in blade count would, however, lead to an increased aerodynamic load on each individual blade which would inevitably raise the risk of non-reattached flow. The suction surface separation bubble in the undisturbed inlet flow case extended over more than 30% surface length and reattachment took place only shortly upstream of the trailing edge. A further increase in blade loading would almost certainly have let to non-reattached flow. Due to the earlier transition and the shorter separated flow regions, the rotor boundary layer in the full stage configuration is less susceptible to complete separation. Thus, the blade load of the investigated high pressure turbine rotor may be increased considerably with respect to a design which is based on the assumption of undisturbed rotor inlet flow. However, as discussed in the introduction, the film cooled first stage HPT rotor airfoils of actual engines may perform differently from the investigated uncooled configuration.

The rotor pressure side boundary layer did not experience significant influences of the passing wakes. Neither the variation of the stator trailing edge coolant ejection, nor the variation of the inter-blade row gap led to a noticeable change in the periodic-unsteady boundary layer transition pattern on the rotor surfaces.

ACKNOWLEDGEMENTS

Parts of the above research were carried out in the course of the European IMT Area 3 Turbine Project AER2-CT-92-0044. The authors gratefully acknowledge the financial support by the CEC.

REFERENCES

Addison, J.S., Hodson, H.P., 1990, "Unsteady transition in an axial flow turbine, Part 1 - Measurements on the turbine rotor"
ASME Journal of Turbomachinery, Vol. 112, pp 206-214.

Bellhouse, B.J., Schultz, D.L., 1966, "Determination of mean and dynamic skin friction, separation and transition in low-speed flow with a thin-film heated element"
Journal of Fluid Mechanics, Vol. 24, Part 2, pp 379-400.

Blair, M.F., Dring, R.P., Joslyn, H.D., 1988, "The effects of turbulence and stator/rotor interactions on turbine heat transfer, Part 1 - Design operating conditions"
ASME Journal of Turbomachinery, Vol. 111, pp 97-103 (1988).

Davies, M.R.D., Byrne, C.M., Dillon, P., 1997, "Instrumentation systems for a continuous flow turbine rotor", ASME Paper 97-GT-315.

Doorly, D.J., Oldfield, M.L.G.:, 1985, "Simulation of the effects of shock wave passing on a turbine rotor blade", ASME Journal of Engineering for Gas Turbines and Power, Vol. 107, pp 998-1006.

Dring, R.P., Joslyn, H.D., Hardin, L.W., Wagner, J.H., 1982, "Turbine rotor-stator interaction"
ASME Journal of Engineering for Power, Vol. 104, pp 729-742.

Guenette, G.R., Epstein, A.H., Giles, M.B., Haimes, R., Norton, R.J.G.:, 1989, "Fully scaled transonic turbine rotor heat transfer measurements"
ASME Journal of Turbomachinery, Vol. 111, pp 1-7.

Halstead, D.E., Wisler, D.C., Okiishi, T.H., Walker, G.J., Hodson, H.P., Shin, H.-W., 1997, "Boundary layer development in axial compressors and turbines" Part 1 of 4 - Composite picture, ASME Journal of Turbomachinery., Vol. 119, pp 114-127.
Part 2 of 4 - Compressors, J. of Turbom., Vol. 119, pp 426-444.
Part 3 of 4 - LP Turbines, J. of Turbom., Vol. 119, pp 225-237.
Part 4 of 4 - Computations and analyses, J. of T., Vol. 119, pp 128-139.

Hodson, H.P., 1983, "The development of unsteady boundary layers on the rotor of an axial-flow turbine", AGARD-CP-351, pp 10-1 - 10-18.

Hodson, H.P., 1985, "Boundary-layer transition and separation near the leading edge of a high-speed turbine blade", ASME Journal of Engineering for Gas Turbines and Power, Vol. 107, pp 127-134 (1985).

Hodson, H.P., 1998, "Bladerow interactions in low pressure turbines" VKI, Lecture series 1998-02.

Hummel, F., 1998, "Validierung des Strömungsberechnungsprogramms "TRACE-U" für eine Hochdruckturbinenstufe", DLR IB 223-98-A 35

Kost, F., Bräunling, W., Schüpferling, E., Göhl, R., 1988, "Detection of separation bubbles by heated thin-film sensors in transonic turbine cascades", 9th Symposium on Measurement Techniques for Transonic and Supersonic Flows in Cascades and Turbomachines, Oxford/England.

Kost, F., Kapteijn, C., 1997, "Application of Laser-Two-Focus velocimetry to transonic turbine flows"
7th International Conference on "Laser Anemometry - Advances and Applications", University of Karlsruhe, Germany.

Mayle, R.E., Dullenkopf, K., 1990, "A theory for wake-induced transition", ASME Journal of Turbomachinery, Vol. 112, pp 188-195.

Pfeil, H., Herbst, R., Schröder, T., 1983, "Investigation of the laminar-turbulent transition of boundary layers disturbed by wakes"
ASME Journal of Engineering for Power, Vol. 105, pp 130-137.

Santoriello, G., Colella, A., Colantuoni, S., 1993, "Rotor blade aerodynamic design", Alfa Romeo Avio, IMT Area 3 turbine project technical report (AER2-CT-92-0044).

Schröder, T., 1991, "Investigations of blade row interaction and boundary layer transition phenomena in a multistage aero engine low-pressure turbine by measurements with hot-film probes and surface-mounted hot-film gauges", VKI, Lecture Series 1991-09.

Schubauer, G.B., Klebanoff, P.S., 1955, "Contributions on the mechanics of boundary-layer transition", NACA TN 3489.

Sharma, O.P., Renaud, E., Butler, T.L., Milaps, K.Jr., Dring, R.P., Joslyn, H.D., 1988, "Rotor-stator interaction in multi-stage axial-flow turbines", AIAA Paper 88-3013.

Tiedemann, M., 1998, "Investigation of the unsteady boundary layer transition in a transonic high pressure turbine stage", Doctoral dissertation, TU Darmstadt; also available as DLR-FB 98-30.

Walker, G.J., 1974, "The unsteady nature of boundary layer transition on an axial-flow compressor blade", ASME Paper 74-GT-135.